Bull. Mater. Sci., Vol. 40, No. 1, February 2017, pp. 79–85. © Indian Academy of Sciences.
DOI 10.1007/s12034-016-1342-4

Effect of Co substitution on the physicochemical properties of $La_{0.67}Sr_{0.22}Ba_{0.11}Mn_{1-x}Co_xO_3$ compounds ($0 \leq x \leq 0.3$)

W CHERIF[1,*], R BEN HASSINE[1], J A ALONSO[2], F J MOMPEÁN[2], M T FERNÁNDEZ-DÍAZ[3] and F ELHALOUANI[4]

[1]Sfax University, Faculty of Sciences, 3000 Sfax, Tunisia
[2]Instituto de Ciencia de Materiales de Madrid, Consejo Superior de Investigaciones Científicas, Cantoblanco, E-28049 Madrid, Spain
[3]Institut Laue-Langevin, F-38042 Grenoble Cedex 9, France
[4]Sfax University, National School of Engineers, 3038 Sfax, Tunisia

MS received 20 December 2015; accepted 25 May 2016

Abstract. **We have prepared a novel series of $La_{0.67}Sr_{0.22}Ba_{0.11}Mn_{1-x}Co_xO_3$ ($0 \leq x \leq 0.3$) perovskites by a sol–gel method. These oxides were characterized by X-ray diffraction (XRD) and neutron powder diffraction (NPD) at room temperature and magnetization measurements *vs*. temperature and various applied magnetic fields. The use of NPD data allows us to describe very precisely the octahedral tilting in the orthorhombic structure (Pnma) observed for all the compounds ($x = 0$ to 0.3); in all the samples with $x > 0$, Co is distributed at random in the Mn positions of the perovskite. Magnetic susceptibility measurements show that whereas the $x = 0$ perovskite is ferromagnetic at relatively high temperatures ($T_C = 360$ K), the introduction of Co induces a magnetic glass state (cluster or spin glass). The magnetic entropy change ($|\Delta S^{max}|$) takes values 2.46, 2.43, 1.88 and 1.78 J kg^{-1} K^{-1} for $x = 0$, 0.1, 0.2 and 0.3, respectively. The relative cooling power is 169, 241, 207 and 191 J kg^{-1} for $x = 0$, 0.1, 0.2 and 0.3, respectively, at a field change of 5 T. This result suggests that subtle Co doping enhances the magnetocaloric effect in this series, the perovskite $La_{0.67}Sr_{0.22}Ba_{0.11}Mn_{0.9}Co_{0.1}O_3$ being a candidate that can be used in magnetic refrigeration.**

Keywords. **Sol–gel; X-ray diffraction; neutron diffraction; Curie temperature; magnetocaloric effect.**

1. Introduction

The term 'manganite' is commonly used to name $REMnO_3$ (RE = trivalent rare-earth ion such as La, Nd and Pr) oxides with ABO_3 perovskite structure. Hole doping is achieved by substituting divalent cations at the RE-site, which converts some of the Mn^{3+} ions (occupying the octahedral B-site) to the Mn^{4+} oxidation state. Hence the general formula of a hole-doped manganite is $RE_{1-x}AE_xMnO_3$ (AE is a divalent alkaline-earth ion such as Ba and Sr). Manganites have been the subject matter of a large number of recent studies due to their interesting structural and magnetic properties, namely the colossal magnetoresistance effect [1]. Doped manganites are ferromagnetic by virtue of a double-exchange (DE) interaction between the trivalent (Mn^{3+}) and tetravalent (Mn^{4+}) ions [2] contained in mixed-valence manganites.

Perovskites with La substituted by cations Sr and Ba were reported to possess appreciable magnetic entropy change with a peak around the Curie temperature (T_C). This fact and the narrow peak profile of the magnetic entropy change *vs*. temperature impose limitations on the usability of these materials for magnetic refrigeration at room temperature [3]. In this context, different scenarios were proposed to modify the peak temperature and broaden the temperature range of the magnetic entropy change, including the substitution of La by a mixture of cations Ba and Sr.

Materials showing sharp ferromagnetic transitions are attractive for magnetic refrigeration applications. Recently, the refrigeration technology has been focused on the magnetic refrigeration based on the magnetocaloric effect (MCE) of a magnetic material because of the potential advantages over gas compression refrigeration [4,5]. The MCE has been studied widely for magnetic refrigeration technology with the aim of suppressing the emission of pollution components that appear in conventional refrigeration systems. The key in using magnetic refrigeration at room temperature is to seek a proper material whose T_C is near room temperature and that can produce a large entropy variation when it goes through a magnetization–demagnetization process [6]. In recent years, extensive attention has been paid to the possibility of room-temperature magnetic refrigeration. Pecharsky and Gschneidner [7] discovered a giant magnetic entropy change associated with the transition temperature (T_C) in Gd metal and then in $Gd_5Si_2Ge_2$ alloy. The last compound exhibits a MCE about twice as large as that exhibited by Gd, the best known magnetic refrigerant material for near-room-temperature applications. However, the purpose in searching a proper material with large magnetic

*Author for correspondence (wajdi_cherif@yahoo.fr)

entropy change and the possibility of application over various temperature ranges always remains.

The MCE takes advantage of the magnetic entropy change; this parameter is well known to achieve relatively high values around the para-to-ferromagnetic transition. We notice that the magnetic entropy change is larger in first-order than in second-order phase transitions, as theoretically predicted and experimentally confirmed. The magnitude of the magnetic entropy change is known to be affected by the microstructure of the material. On the other hand, the relative cooling power (RCP) depends also on the width of transition temperature interval [4,5]. The third important factor for the applicability of materials is the critical temperature of the transition, which may be tuned mainly by a chemical composition.

The MCE has been recently studied in manganites [8–10], either pristine $RE_{1-x}AE_xMnO_3$ or containing some transition metals (Fe, Co, Ni,. . .) partially replacing Mn ions. Some studies have discussed the effect of Co doping on the structural and magnetic properties. Such manganites have a complex band structure containing trivalent Mn^{3+} and trivalent Co^{3+} ions occupying at random the octahedral (B) sites [11,12]. As a rule of thumb, the substitution of Co ions by Mn ions in $RE_{1-x}AE_xMn_{1-x}Co_xO_3$ manganites introduces lattice distortions but also reduces the Mn^{3+}/Mn^{4+} ratio, affecting double exchange and magnetic interactions.

The aim of this work is the study of the effect of the partial replacement of Mn ions by Co ions on the structural (including neutron diffraction studies) and magnetic properties of $La_{0.67}Sr_{0.22}Ba_{0.11}Mn_{1-x}Co_xO_3$ ($x = 0$, 0.1, 0.2 and 0.3) perovskites, with particular emphasis on the MCE; we describe an enhancement of the RCP for moderate Co-doping levels.

2. Experimental

Polycrystalline $La_{0.67}Sr_{0.22}Ba_{0.11}Mn_{1-x}Co_xO_3$ ($x = 0$, 0.1, 0.2 and 0.3) samples were synthesized by the sol–gel method from $MnCO_3$, La_2O_3, $SrCO_3$, $BaCO_3$ and Co_2O_3 (99.9% purity) in the appropriate stoichiometric proportions. The powders were dissolved in nitric acid, HNO_3. Suitable amounts of citric acid and ethylene glycol as a chelating agent were added until a completely homogeneous and transparent solution was achieved. After slowly drying the solution, it was decomposed at 600°C in air. Finally, the resulting powders were annealed in air at 1000°C.

The structure, phase purity and homogeneity of the as-elaborated samples were checked by X-ray powder diffraction (XRD) using CuKα radiation ($\lambda = 1.54056$ Å) and neutron powder diffraction (NPD). The crystallographic structures were refined from high-resolution NPD patterns collected at the Institut Laue-Langevin (ILL) in Grenoble (France), acquired at room temperature using the D2B diffractometer with $\lambda = 1.594(1)$ Å. About 3 g of each sample was contained in vanadium cylinders; the counting time was 2 h for each data collection in the high-intensity mode. The diffraction data were analysed by the Rietveld method using the FULLPROF program [13] and the average particle size was determined using the Scherrer formula [14]. A pseudo-Voigt function was chosen to generate the line shape of the diffraction peaks. The background was approximated with a 5th-degree polynomial. The following parameters were refined in the final runs: scale factor, background coefficients, zero-point error, pseudo-Voigt corrected for asymmetry parameters, positional coordinates, isotropic displacement factors and mixed occupancy factors of Mn/Co. The coherent scattering lengths for La, Sr, Ba, Mn, Co and O were 8.240, 7.02, 5.07, −3.73, 2.49 and 5.805 fm, respectively.

Magnetic measurements were performed on a commercial SQUID magnetometer from Quantum Design; the *dc* magnetic susceptibility was recorded in the temperature range 5–450 K in ZFC and FC runs with an applied field of 0.1 T with a heating rate of 5 K min^{-1}; magnetization isotherms were collected between −50 and +50 kOe with $\Delta T = 8$ K between 300 and 420 K ($x = 0$), 238 and 358 K ($x = 0.1$), 158 and 286 K ($x = 0.2$) and 126 and 254 K ($x = 0.3$). The magnetic entropy changes $|\Delta S_M|$ were estimated from the magnetization data using a Maxwell relation.

3. Results and discussion

3.1 *Crystallographic structure*

The results of XRD indicate that the four compounds are single-phase perovskite manganites. Supplementary figure S1a–d shows typical perovskite X-ray patterns for the four samples, displaying single structure without any other secondary or impurity phase. The four diagrams are Rietveld refined with the model developed from NPD data (figure 1 and supplementary figure S2b–d). From XRD data it is difficult to determine any deviation from the cubic symmetry, since the structural distortion is weak and the superstructure reflections are almost invisible; hence NPD is required.

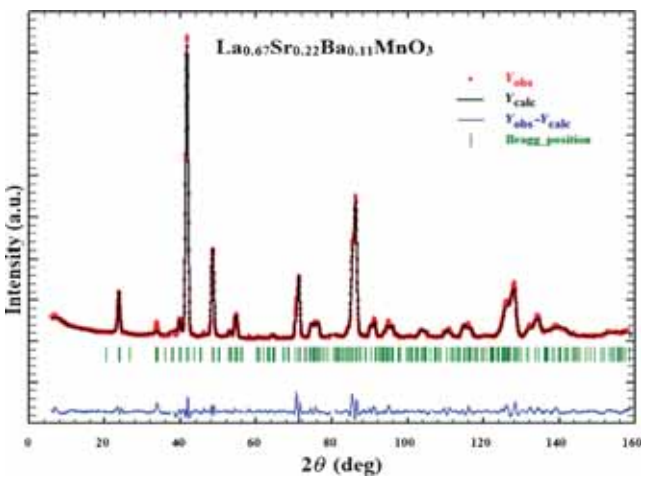

Figure 1. Observed (crosses), calculated (full line) and difference (bottom) NPD rietveld profiles for $La_{0.67}Sr_{0.22}Ba_{0.11}Mn_{0.9}Co_{0.1}O_3$ at 298 K. Vertical lines correspond to the Bragg positions.

The NPD analysis for $La_{0.67}Sr_{0.22}Ba_{0.11}Mn_{1-x}Co_xO_3$ ($0 \leq x \leq 0.3$) helped assessing the true symmetry and structural features of these oxides. NDP patterns can be indexed in the orthorhombic system with Pnma space group for the four samples. With cobalt doping no structural changes were identified. The structural analysis indicated that La, Sr and Ba are distributed at random over the 4*c* (x,1/4,z) positions, Mn and Co atoms occupy, at random, a single position at 4*b* (0,0,1/2) Wyckoff sites, and there are two independent positions for oxygen atoms, O1 (4*c*) and O2 (8*d*). In table 1 we list the refined unit-cell parameters and atomic positions for all samples. After the simultaneous refinement of all the variable parameters, we obtained good values of the discrepancy R_p, R_{wp}, R_{exp}, R_{Bragg} and χ^2 parameters, also included in table 1. Some selected interatomic distances (Mn–O bond distances) and Mn–O–Mn bond angles are listed in table 2.

Table 1. Unit-cell, positional and thermal parameters and discrepancy factors after the refinement of the crystal structure from NPD data at RT of $La_{0.67}Sr_{0.22}Ba_{0.11}Mn_{1-x}Co_xO_3$. Crystallite size is also included.

Co content (x)	0	0.1	0.2	0.3
Space group	Pnma	Pnma	Pnma	Pnma
Cell parameters				
a (Å)	5.4590(6)	5.4682(4)	5.4637(7)	5.4582(5)
b (Å)	7.7174(7)	7.7657(6)	7.7453(1)	7.7452(7)
c (Å)	5.5273(2)	5.5139(6)	5.5158(3)	5.5023(5)
V (Å^3)	232.86(7)	234.39(7)	233.42(1)	232.60(8)
Atomic position				
La/Ba/Sr 4*c* (x,1/4,z)				
x	−0.0001(5)	–0.001(2)	0.002(5)	0.0046(7)
z	−0.0028(5)	0.0010(1)	−0.0040(6)	0.0006(8)
B (Å^2)	0.76(7)	0.46(6)	0.33(1)	0.29(5)
Mn/Fe4*b* (0,0,1/2)				
B (Å^2)	0.03(6)	0.49(1)	0.08(1)	0.66(1)
O1 4*c* (x,1/4,z)				
x	0.509(4)	0.508(3)	0.495(5)	0.488(2)
z	0.0401(1)	0.0495(9)	0.0496(6)	0.0477(7)
B (Å^2)	0.51(4)	0.07(1)	0.33(9)	0.60(8)
O2 8*d* (x,y,z)				
x	0.2613(1)	0.2602(1)	0.254(3)	0.251(3)
y	0.0194(6)	0.0178(6)	0.0167(4)	0.0172(4)
z	0.747(4)	0.754(4)	0.748(3)	0.751(3)
B (Å^2)	0.65(6)	1.55(4)	1.26(2)	1.32(6)
Discrepancy factors (%)				
R_p	18.3	17.4	11.1	12.7
R_{wp}	17.7	14.4	8.66	10.0
R_{exp}	4.32	5.65	5.90	5.84
χ^2	16.8	6.54	2.16	2.46
R_{Bragg}	5.65	4.02	1.74	2.93
Crystallite size				
D (nm)	32.31	26.8	22.19	26.97

Table 2. Main bond distances (Å) and selected angles (deg) for $La_{0.67}Sr_{0.22}Ba_{0.11}Mn_{1-x}Co_xO_3$ at RT.

Co content (x)	0	0.1	0.2	0.3
Bond distances				
Mn–O1	1.9299(3)	1.9610(8)	1.9557(6)	1.9551(7)
Mn–O2	1.911(2)	1.892(17)	1.938(16)	1.934(16)
Mn–O2	1.989(2)	2.001(17)	1.953(16)	1.950(16)
⟨Mn–O⟩	1.943	1.951	1.949	1.946
Angles				
Mn–O1–Mn	166.58(5)	163.79(4)	163.84(3)	164.09(3)
Mn–O2–Mn	170.4(7)	171.7(7)	172.3(7)	172.1(7)
⟨Mn–O–Mn⟩	169.13	169.06	169.48	169.43

The quality of the fit of observed and calculated NDP profiles after the Rietveld refinements are displayed in figure 2. No extra peaks were detected in the NPD patterns that could indicate the presence of impurities in the samples.

Figure 2 shows a view of the crystal structure. The orthorhombic distortion of the perovskite, described in the Pnma space group, of $La_{0.67}Ba_{0.22}Sr_{0.11}Mn_{1-x}Co_xO_3$ oxides at room temperature gives rise to the tilting of the $(Mn,Co)O_6$ octahedra in order to optimize the (La,Ba,Sr)–O distances.

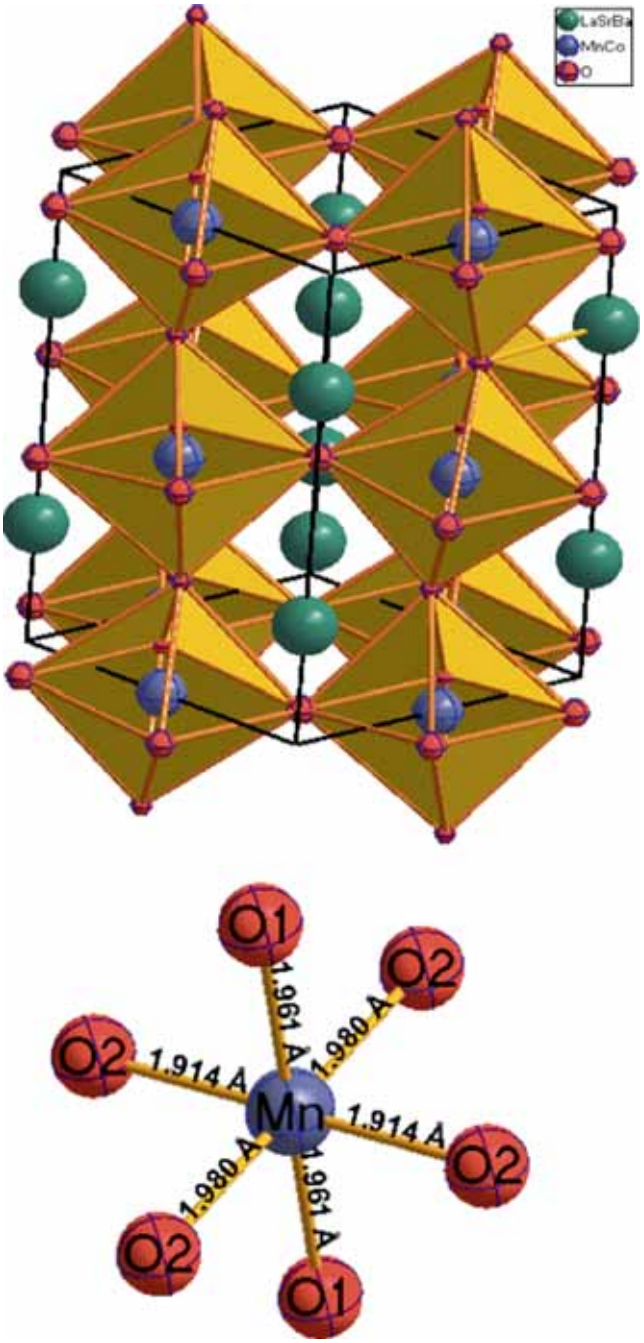

Figure 2. View of the orthorhombic (Pnma) crystal structure of $La_{0.67}Sr_{0.22}Ba_{0.11}MnO_3$ and the coordination polyhedron of Mn displaying the Mn–O distances.

The $(Mn,Co)O_6$ octahedra are almost regular, showing a slight distortion as observed in a previous work [15].

Supplementary figure S3a exhibits the variation of unit-cell volume and $\langle dMn–O_1 \rangle$ bond distances and supplementary figure S3b the $\langle Mn–O_1–Mn \rangle$ bond angles as a function of cobalt content. From $x = 0$ to 0.1 there is a considerable increase of the unit-cell volume, and then a gradual decrease of V for a further increment of the Co concentration. This is not easily deduced from the similarity in ionic radii between Co^{3+} (0.61 Å) and Mn^{3+} (0.645 Å) in sixfold coordination and high-spin state for both cations [16]. For low doping levels we can speculate that the introduction of Co^{3+} decreases the effectiveness of the hole doping effect given by the replacement of 33% La by alkali-earth ions, leading to a lower content of Mn^{4+} in the $x = 0.1$ Co-doped sample, showing a larger unit-cell volume and $\langle (Mn,Co)–O \rangle$ distances. For further Co doping, the smaller ionic radius of Co^{3+} seems to predominate in the cell volume as well as in the $\langle (Mn,Co)–O \rangle$ distances. The Pnma space group involves $a^-b^+c^-$ tilting of the octahedra (in antiphase along the a and c directions of the aristotype, and in phase along the long b-axis direction). The marked increase of the $\langle (Mn,Co)–O \rangle$ distances for $x = 0.1$ (supplementary figure S3a) drives a concomitant decrease of the tolerance factor of the perovskite, thus implying a more serious rotation of the $(Mn,Co)O_6$ octahedra. This structural effect should decrease the superexchange Mn–O–Mn angles (supplementary figure S3b), reducing the overlap between (Mn,Co)3d and O2p orbitals and thus perturbing the magnetic interactions. As expected, for $x = 0.1$ a minimum Mn–Ô–Mn angle is observed (supplementary figure S3b).

The average crystallite size was estimated from the NDP data using the Scherer relation [14]

$$D = \frac{K\lambda}{\beta \cos\theta}.$$

Here K, β, λ and θ are the grain shape factor, the X-ray wavelength, the full-width at half-maximum (FWHM) of the diffraction peak and the Bragg diffraction angle, respectively. The values of the effective crystallite sizes are summarized in table 1. In all cases a nanometric size for the crystallites is found, around 30 nm, which is related to the moderate synthesis temperatures of these samples, of 1000°C, obtained from very reactive precursors from sol–gel procedures.

3.2 *Magnetic properties*

Figures 3 and 4 show both the zero-field-cooled (ZFC) and field-cooled (FC) curves of the $La_{0.67}Sr_{0.22}Ba_{0.11}Mn_{1-x}Co_xO_3$ samples, with the Co content in the $0 \leq x \leq 0.3$ range, obtained under a magnetic field of 0.1 T. They all show a spontaneous increase of the magnetization below Curie temperatures, T_C, which are defined as the inflection point in the $M–T$ curves (see the inset of figure 5). Both the magnetization and T_C decrease with increasing Co content; T_C values are gathered in table 1. For $x = 0$, the thermal variation of the susceptibility is characteristic of a

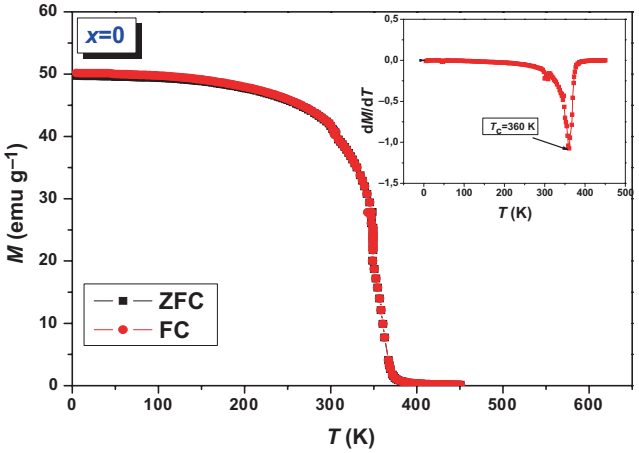

Figure 3. Temperature dependence of ZFC and FC magnetization data taken at $H = 1000$ Oe for $x = 0$; the inset represents dM/dT *vs.* T curves, to determine T_C.

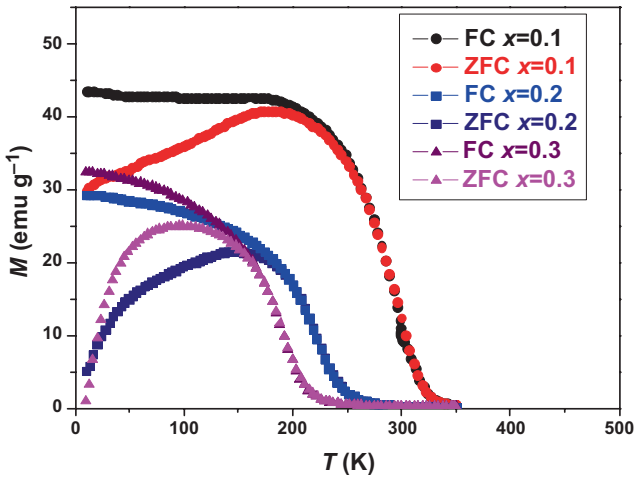

Figure 4. Temperature dependence of ZFC and FC magnetization data taken at $H = 1000$ Oe for $x = 0.1$, 0.2 and 0.3.

paramagnetic (PM) to ferromagnetic (FM) phase transition as temperature decreases below $T_C = 360$ K; both FC and ZFC curves are superposed in all the temperature ranges. For $x = 0.1$, T_C decreases down to 300 K and a divergence between FC and ZFC curves is observed. The magnetizations are more markedly reduced for $x = 0.2$ and 0.3. The history dependence of the magnetization processes indicated by the bifurcation between ZFC and FC is still more dramatic for $x = 0.2$ and 0.3 at low temperature. This may be due to the appearance of a spin-glass (SG) state induced by the competition between FM and AFM exchange interactions. From these data it is evident that the presence of Co at the octahedral position strongly perturbs the double exchange mechanism between Mn^{3+} and Mn^{4+} ions, inducing competitive antiferromagnetic superexchange interactions of the type Co^{3+}–O–Mn^{3+} or Co^{3+}–O–Mn^{4+}. This competition may lead to a frustrated spin arrangement or a severe canting of the magnetic moments in non-collinear magnetic structures; both scenarios give rise to the observed

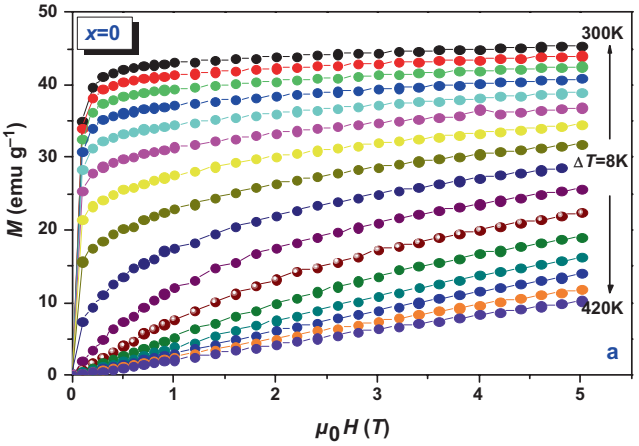

Figure 5. Magnetization *vs.* field isotherms near T_C for the $La_{0.67}Sr_{0.22}Ba_{0.11}MnO_3$ sample.

divergence between ZFC and FC curves and the reduction of the magnetic ordering temperature.

Karmakar *et al* [17] showed that the substitutions at the Mn site with ions having stable electronic configuration such as Fe, Ga and Mg [18] are more prone to induce spin-glass states, whereas substitutions with ions showing multiple valence such as Co, Ni and Ru [19] promote the formation of magnetic clusters and spin freezing in the system.

3.3 *MCE*

Figure 5 and supplementary figure S4b–d show isothermal magnetization curves for $La_{0.67}Sr_{0.22}Ba_{0.11}Mn_{1-x}Co_xO_3$ samples ($0 \leq x \leq 0.3$), measured under applied magnetic fields ranging between 0 and 5 T and at temperatures spanning from 300 to 420 K ($x = 0$), 238 to 358 K ($x = 0.1$), 158 to 286 K ($x = 0.2$) and 126 to 254 K ($x = 0.3$). The isothermal magnetization $M(H, T)$ magnetic field dependency, measured at different temperatures below T_C, shows a non-linear behaviour with a sharp increase for low field values and a tendency to saturate as the magnetic field increases, reflecting a ferromagnetic behaviour. Beyond the Curie temperature, the material follows a paramagnetic behaviour in which the ferromagnetic order is broken, due to the random reorientation of the magnetic moments caused by thermal agitation [20].

We determined from the $M(H)$ isotherms the temperature dependence of $|\Delta S_M|$.

Figure 6 and supplementary figure S5b–d show the magnetic entropy change $|\Delta S_M|$ for the four samples as a function of temperature under different magnetic fields: 1, 2, 3, 4 and 5 T.

From the $M(HT)$ data, the magnetic entropy change for our samples can be calculated as [21]

$$\Delta S_M(T, \Delta H) = S_M(T, H) - S_M(T, 0) = \int_0^H \left(\frac{\partial M}{\partial T}\right)_H dH. \quad (1)$$

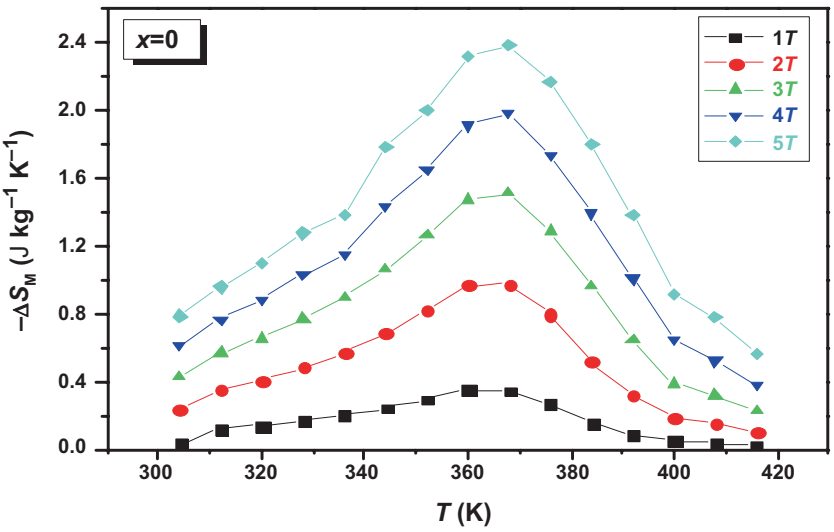

Figure 6. Thermal evolution of the entropy under different amplitudes of change in the magnetic field (from bottom to top, ΔH = 1, 2, 3, 4 and 5 T) for the $La_{0.67}Sr_{0.22}Ba_{0.11}MnO_3$ sample.

Table 3. Comparison of Curie temperature (T_C), maximum entropy change ΔS_M^{max} and RCP for $La_{0.67}Sr_{0.22}Ba_{0.11}Mn_{1-x}Co_xO_3$ based materials.

Samples	T_C (K)	ΔS_M^{max} (J kg^{-1}K^{-1})	RCP (J kg^{-1})	ΔH (T)	Ref
Gd	294	10.2	410	5	[21]
$La_{0.67}Sr_{0.22}Ba_{0.11}MnO_3$	360	2.46	169	5	This work
$La_{0.67}Sr_{0.22}Ba_{0.11}Mn_{0.9}Co_{0.1}O_3$	300	2.41	242	5	This work
$La_{0.67}Sr_{0.22}Ba_{0.11}Mn_{0.8}Co_{0.2}O_3$	220	1.88	207	5	This work
$La_{0.67}Sr_{0.22}Ba_{0.11}Mn_{0.7}Co_{0.3}O_3$	185	1.78	191	5	This work
$La_{0.7}Ca_{0.2}Sr_{0.1}Mn_{0.9}Cr_{0.1}O_3$	255	3.8	240	5	[5]
$La_{0.7}Sr_{0.3}Mn_{0.9}Al_{0.1}O_3$	310	2.6	109	5	[6]
$La_{0.67}Ca_{0.33}MnO_3$	252	2.06	175	5	[7]
$La_{0.67}Ba_{0.33}MnO_3$	292	1.48	161	5	[7]
$La_{0.67}Sr_{0.33}MnO_3$	348	1.69	211	5	[7]
$Gd_5(Si_2Ge_2)$	275	18.5	535	5	[21]

In the case of magnetization measurements at small discrete fields and temperature intervals, the numerical approximation of the integral in equation (1) could be approximated as [22]

$$\Delta S_M(T, \Delta H) = \sum \frac{M_i - M_{i+1}}{T_i - T_{i+1}} \Delta H_i, \qquad (2)$$

where M_i and M_{i+1} are, respectively, the experimental data of the magnetization at T_i and T_{i+1}, under a magnetic field H_i.

In figures 6 and supplementary figure S5b–d, we observe that $|\Delta S_M|$ increases with an increasing applied magnetic field. The maximum entropy change corresponding to a magnetic field at 5 T for these samples is presented in table 3.

The magnetic cooling efficiency of a magnetocaloric material is evaluated by considering the RCP [6] given by

$$RCP = |\Delta S_M^{max}| \times \delta T_{FWHM},$$

where $|\Delta S_M^{max}|$ is the maximum entropy change at T_C and $\delta T_{FWHM} = (T_2 - T_1)$ is the full-width temperature span of the $|\Delta S_M|$ *vs.* temperature plots at their half-maxima. The RCP values for x = 0, 0.1, 0.2 and 0.3 samples exhibit an almost linear rise with increasing field, as shown in figure 7. For a 5 T field change, the RCP values are presented in table 3. To evaluate the applicability of $La_{0.67}Sr_{0.22}Ba_{0.11}Mn_{1-x}Co_xO_3$ samples ($0 \leq x \leq 0.3$) as magnetic refrigerants, the values of $|\Delta S^{max}|$ and RCP obtained in our study were compared with those reported in the literature for several other magnetic materials (table 3). It is noteworthy that our RCP values for x = 0, 0.1, 0.2 and 0.3 samples are, respectively, about 41, 59, 51 and 46% of that of pure Gd [23] under $\Delta H = 5$ T. The RCP of $La_{0.67}Sr_{0.22}Ba_{0.11}Mn_{0.9}Co_{0.1}O_3$ compound is higher than those obtained by Nam *et al* [9] and similar to that of $La_{0.67}Sr_{0.22}Ba_{0.11}MnO_3$ reported by Morelli *et al* [10]. Figure 7 shows that the RCP values of all the Co-doped perovskites are superior to that of the parent undoped compound

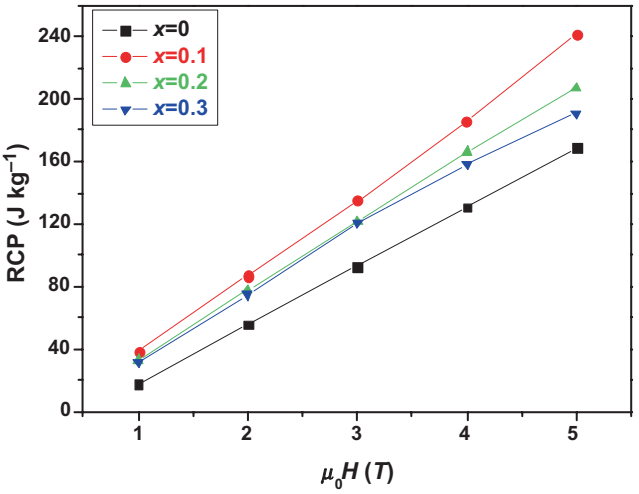

Figure 7. Relative cooling power values (RCP) *vs.* applied magnetic field for $La_{0.67}Sr_{0.22}Ba_{0.11}Mn_{1-x}Co_xO_3$ ($0 \leq x \leq 0.3$) compounds.

in all the magnetic field ranges; however it is interesting to notice that RCP reaches a maximum for $x = 0.1$ Co doping level; for this composition, with T_C still around room temperature, the sharpness of the ferromagnetic transition makes it a potential candidate competitive with state-of-the-art conventional refrigerant materials (table 3).

4. Conclusion

In this work we investigated the structural, magnetic and magnetocaloric properties of nanopowder samples $La_{0.67}Sr_{0.22}Ba_{0.11}Mn_{1-x}Co_xO_3$ prepared by sol–gel method and sintered at 1000°C, yielding nanometric powders. Neutron diffraction was useful in investigating subtle structural features; NPD data show that all the samples crystallize in the orthorhombically distorted perovskite structure with Pnma space group; the most distorted crystal structure is observed for $x = 0.1$, with a lower tolerance factor due to the longest (Mn,Co)–O distances across the series. Magnetic measurements show a ferromagnetic behaviour for $x = 0$, whereas compounds with $x \geq 0.1$ present a divergence of FC *vs.* ZFC susceptibility curves magnetic due to the appearance of antagonistic antiferromagnetic interactions upon introduction of Co^{3+} moments, which compete with the double exchange effect associated with the mixed $Mn^{3+,4+}$ valence. The RCP is 169, 241, 207 and 191 J kg^{-1} for the samples $x =$ 0, 0.1, 0.2 and 0.3 under $\Delta H = 5$ T, respectively. Hence, the compound doped with Co ($x = 0.1$) is a candidate for refrigerant magnetic compared with those of some others manganites with related compositions or prepared by other methods.

Acknowledgements

We acknowledge the financial support of the Spanish Ministry of Economy and Competitivity through projects MAT2013-41099-R and MAT2011-27470-C02-02. We are grateful to ILL for making all facilities available.

Electronic supplementary material

Supplementary material pertaining to this article is available on the *Bulletin of Materials Science* website (www.ias.ac.in/matersci).

References

[1] Von Helmolt R, Wecker J, Holzapfel B, Schultz L and Samwer K 1993 *Phys. Rev. Lett.* **71** 2331

[2] Zener C 1951 *Phys. Rev.* **81** 440

[3] Zhong W, Au C T and Du Y W 2013 *Chin. Phys. B* **22** 11-057501

[4] Phan M H and Yu S C 2007 *J. Magn. Magn. Mater.* **308** 325

[5] Szymczak R, Czepelak M, Kolano R, Kolano-Burian A, Krzymańska B and Szymczak H 2008 *J. Mater. Sci.* **43** 1734

[6] Phan M H and Yu S C 2007 *J. Magn. Magn. Mater.* **308** 325

[7] Pecharsky V K and Gschneidner Jr K A 1997 *Phys. Rev. Lett.* **78** 4494

[8] Dhahri Ah, Jemmali M, Taibi K, Dhahri E and Hlil E K 2015 *J. Alloys Compd.* **618** 488

[9] Nam D N H, Nguyen V D, Hong L V, Phuc N X, Yu S C, Tachibana M and Takayama-Muromachi E 2008 *J. Appl. Phys.* **103** 043905

[10] Morelli D T, Mance A M, Mantese J V and Micheli A L 1996 *J. Appl. Phys.* **79** 373

[11] Rao G H, Sun J R, Kattwinkel A, Haupt L, Baerner K, Schmitt E and Gmelin E 1999 *Physica B* **269** 379

[12] Sugantha M, Singh R S, Guha A, Raychaudhuri A K and Rao C N R 1998 *Mater. Res. Bull.* **33** 1129

[13] Rodríguez-Carvajal J 1993 *Physica B* **192** 55

[14] Guinier A 1964 In: *Théorie et technique de la radiocristallographie*, X Dunod (ed) 3rd edn p 482

[15] Ellouze M, Boujelben W, Cheikhrouhou A, Fuess H and Madar R 2002 *Solid State Commun.* **124** 125

[16] Shannon R D 1976 *Acta Crystallogr. A* **32** 751

[17] Karmakar S, Taran S, Chaudhuri B K, Sakata H, Sun C P, Huang C L and Yang H D 2006 *Phys. Rev. B* **74** 104407

[18] Tan S, Yue S and Zhang Y 2003 *Phys. Lett. A* **319** 530

[19] Pal S, Bose E, Chaudhuri B K, Yang H D, Neeleshwar S and Chen Y Y 2005 *J. Magn. Magn. Mater.* **293** 872

[20] Arayedh B, Kallel S, Kallel N and Peña O 2014 *J. Magn. Magn. Mater.* **361** 68

[21] Bohigas X, Tejada J, Martinez-Sarrión M L, Tripp S and Black R 2000 *J. Magn. Magn. Mater.* **208** 85

[22] McMichael R D, Ritter J J and Shull R D 1993 *J. Appl. Phys.* **73** 6946

[23] Pecharsky V K, Gschneidner K A and Tsokol A O 2005 *Rep. Prog. Phys.* **68** 1479